ARL-TR-9306 ● SEP 2021

DEVCOM ARMY RESEARCH LABORATORY

An In-Depth Investigation of the Effect of Curing Temperature on Spiropyran Mechanophore Activation in Bulk PDMS under Dynamic Loading

by James Berry, Logan Shannahan, Stephen Craig, and Müge Fermen-Coker

NOTICES

Disclaimers

The findings in this report are not to be construed as an official Department of the Army position unless so designated by other authorized documents.

Citation of manufacturer's or trade names does not constitute an official endorsement or approval of the use thereof.

Destroy this report when it is no longer needed. Do not return it to the originator.

ARL-TR-9306 ● SEP 2021

An In-Depth Investigation of the Effect of Curing Temperature on Spiropyran Mechanophore Activation in Bulk PDMS under Dynamic Loading

James Berry, Logan Shannahan, and Müge Fermen-Coker
Weapons and Materials Research Directorate,
DEVCOM Army Research Laboratory

Stephen Craig
Duke University

REPORT DOCUMENTATION PAGE		Form Approved OMB No. 0704-0188

1. REPORT DATE *(DD-MM-YYYY)*	2. REPORT TYPE	3. DATES COVERED (From - To)
September 2021	Technical Report	January 2020–August 2021

4. TITLE AND SUBTITLE
An In-Depth Investigation of the Effect of Curing Temperature on Spiropyran Mechanophore Activation in Bulk PDMS under Dynamic Loading

5a. CONTRACT NUMBER

5b. GRANT NUMBER

5c. PROGRAM ELEMENT NUMBER

6. AUTHOR(S)
James Berry, Logan Shannahan, Stephen Craig, and Müge Fermen-Coker

5d. PROJECT NUMBER

5e. TASK NUMBER

5f. WORK UNIT NUMBER

7. PERFORMING ORGANIZATION NAME(S) AND ADDRESS(ES)
DEVCOM Army Research Laboratory
ATTN: FCDD-RLW-TC
Aberdeen Proving Ground, MD 21005

8. PERFORMING ORGANIZATION REPORT NUMBER
ARL-TR-9306

9. SPONSORING/MONITORING AGENCY NAME(S) AND ADDRESS(ES)

10. SPONSOR/MONITOR'S ACRONYM(S)

11. SPONSOR/MONITOR'S REPORT NUMBER(S)

12. DISTRIBUTION/AVAILABILITY STATEMENT
Approved for public release: distribution unlimited.

13. SUPPLEMENTARY NOTES
ORCID IDs: Stephen Craig, 0000-0002-8810-0369; Müge Fermen-Coker, 0000-0001-9370-2586. This report has been edited per the style guide *Scientific Style and Format: The CSE Manual for Authors, Editors, and Publishers*. 8th ed. University of Chicago Press; 2014.

14. ABSTRACT
Embedded in the silicone elastomer polydimethylsiloxane (PDMS), the spiropyran mechanophore mechanochemically changes color under applied load, linking molecular-level behavior to macro-scale loading. As the spiropyran is covalently linked to the PDMS polymer chain, the mechanical properties of the silicone elastomer substrate play a large role in the material's behavior and timing of mechanochromism. Here, the influence of the PDMS curing temperature on material behavior and mechanochromic response of the embedded spiropyran is studied under uniaxial dynamic compression at rates of 1000 s^{-1}. Higher curing temperatures are shown to produce stiffer material, which requires increased stress to initiate color change. However, a consistent onset strain of approximately 90% is needed, regardless of stress. These results suggest activation is strain controlled, and that increasing cross-linking density, coupled with the corresponding reduction in stretchability, increases the force required to reach a consistent activation strain.

15. SUBJECT TERMS
mechanochemistry, high-rate characterization, spiropyran, Kolsky bar, polydimethylsiloxane, PDMS, curing temperature, stress–strain

16. SECURITY CLASSIFICATION OF:			17. LIMITATION OF ABSTRACT	18. NUMBER OF PAGES	19a. NAME OF RESPONSIBLE PERSON
a. REPORT	b. ABSTRACT	c. THIS PAGE			James Berry
Unclassified	Unclassified	Unclassified	UU	23	19b. TELEPHONE NUMBER (Include area code) 410-278-1519

Contents

List of Figures

List of Tables

1. Introduction

Over the past few decades, mechanophores, force-sensitive molecules that contain a labile bond, have demonstrated the ability to change the properties of a polymeric material in which they are embedded, potentially leading to a variety of unique applications. While much early research on mechanophores focused on polymers in the solution phase,[1] recent developments focused on mechanophores placed into bulk materials. Potential uses for these molecules in the bulk phase include damage detection,[2] force sensing,[3] self-healing,[4] acid generation,[5] and controlled small-molecule release.[6] Using spiropyran (SP) mechanophores, our group showed the first example of the visualization of molecular-level bond breakage during standard high-rate material characterization experiments, prior to the onset of macroscopic damage.[7] This was an important achievement because it displayed the ability to bridge the length scales, from molecular to macroscopic, during high-rate material characterization.

An important topic of research for the Army is the tuning of materials that respond to their environment "at the speed of fight". These embedded mechanophores enable a material to rapidly respond to an outside stimulus such as force and turn a negative outcome, such as chain scission, into a positive one, such as the ability to prevent and/or repair material failure to increase the resistance of the material to blast and penetration loadings. Several parameters of SP-polydimethylsiloxane (PDMS) samples have been investigated in the literature with varying degrees of effect on the force necessary for activation to the colored merocyanine (MC). Regiochemical isomers with differing connections to the PDMS backbone were investigated and shown to have a negligible effect on mechanophore activation during both quasi-static[8] and high-rate loading.[9] Functional group substitution on the mechanophore itself has also been studied and significant changes were observed during atomic force microscopy studies.[10] When cured into a bulk polymer, the electron-withdrawing nitro ($-NO_2$) group produced a significant positive effect on mechanophore activation.[9] These two parameters—attachment point to the SP and functional group substitution—show that aside from the highly electron-withdrawing nitro group, variation around the small-molecule SP mechanophore itself does not influence mechanophore activity to a significant extent. Increased branching of the connections between the mechanophore and the bulk material has influenced activation, with stiffer materials requiring less force[11] for activation than softer elastomeric materials[12] when compared with the linear counterparts. Alternatively, altering the ratio of bulk elastomer to curing agent influenced mechanophore activity in bulk PDMS. The larger the ratio of bulk elastomer to curing agent, the larger the distance between cross links and, thus, a

softer material was produced that required higher strains to achieve activation.[13] Taken together, these studies show that while functional group variation on the SP itself produces a negligible effect (with the exception of strongly electron-withdrawing groups), molecular architecture (branching) and bulk material properties can provide a significant influence on mechanophore activity in these systems.

The contact angle of water droplets on the surface of PDMS is influenced by the curing temperature of the PDMS sample itself. During the process of curing at different temperatures, a complex interplay among Si-H, Si-OH, and Si-O-Si from autoxidation influences the hydrophobicity/hydrophilicity of the PDMS surface.[14] This observed change in bulk properties of PDMS provided an inspiration to apply a similar temperature variation to examine the effect curing temperature may have on the bulk properties of SP-embedded PDMS and its behavior under high-rate loading conditions. Johnson found that increasing the curing temperature causes a linear decrease in the compressive modulus,[15] but the PDMS in that study did not include embedded mechanophores. Varying the curing temperature parameter could provide a method of tuning the mechanophore response for activation at different levels of applied force. This would have important implications to the Army because protection materials that require a stress–strain reporting capability could be tuned to their specific application.

The curing temperature can influence cross-link density in the final PDMS system.[16] In a system such as Sylgard-184 (Dow Corning), the activity of the catalyst is influenced by the temperature at which the sample is cured, with higher temperatures corresponding to increased catalytic activity. With greater catalytic activity, more cross links in the bulk system can be formed, which will increase the stiffness of the final sample. In fact, it was shown in a glassy poly(methyl methacrylate) (PMMA) system that an increase in cross-link density can necessitate a corresponding increase in stress to produce the requisite color change activation of cross-linked SP under uniaxial tension, until a saturation threshold is reached.[17] To study if this same trend can be shown in soft materials, we varied the temperature at which the SP-embedded specimen was cured into bulk PDMS. Here, we disclose the results of high-rate characterization of SP-embedded PDMS cured at four different temperatures (23, 68, 113, and 138 °C), and we report our findings on the effect that curing temperature has on mechanophore activation in bulk PDMS.

2. Sample Preparation

2.1 Chemistry

The chemistry employed in the synthesis of SP-NO_2 **1** (Fig. 1) was reported previously (see Appendix for detailed synthetic procedures).[7,9,18,19]

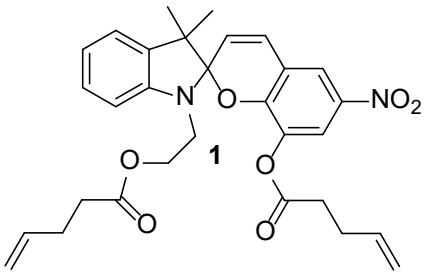

Fig. 1 Functionalized SP-NO_2 1 used in this study

2.2 Curing

It has been shown that the cross-link density within a sample would influence its mechanochromic activity.[13,17] Since the temperature at which the PDMS sample is cured will influence the cross-link density, a range of curing temperatures were chosen: 23 °C (room temperature [RT]), 68 °C (typical curing temperature for SP-PDMS samples), 113 °C, and 138 °C. Sylgard-184 was used as the commercial PDMS bulk material for these experiments. A similar process to that previously reported for curing cylindrical samples was used in this work[7]; the major difference in the present work is the temperature of the oven during curing. Samples were mixed and degassed under vacuum as usual and then removed from the vacuum oven. The oven was then preheated to the desired temperature and the sample mold placed into the oven for isothermal overnight curing. A total of five PDMS cylinders embedded with SP-NO_2 **1** were produced for each temperature, from which three or four Kolsky samples could be cut from each cylinder.

3. Testing

PDMS samples at the four examined curing temperatures were tested on a compression Kolsky bar. Samples were prepared by cutting individual cylinders from the molded feedstock to a nominal length of 4.8 mm, and a diameter, as molded, of 6.1 mm. The length was chosen as a compromise between the necessities of ensuring a uniform stress state in the sample during the experiment and ensuring the sample is of sufficient length to enable quality high-speed imagery. To ensure cuts were perpendicular to the loading axis and parallel to each

other, a constructed jig was used in which the sample stock was held in a tube with an inner diameter comparable to the sample to prevent bending or other deformation of the sample during the cutting process. A razor blade lubricated with mineral oil was used to slice the sample through a gap in the tube. Despite these precautions, minor deflection occurred during cutting, especially in the softer RT cure samples.

As PDMS is too soft in comparison with typical steel and aluminum bars, polycarbonate bars were used, resulting in larger bar strains and larger strain signals. However, as polycarbonate is a viscoelastic material, a viscoelastic correction code was implemented following the methodology described by Bacon.[20] This is necessary as the underlying assumptions of Kolsky analysis assume an elastic material. The viscoelastic correction method also takes into account and removes dispersion effects, such that the corrected data can be treated as a 1-D wave propagation problem as in typical Kolsky analysis. During the experiments, mineral oil was used to lubricate the bar/sample interfaces and reduce friction effects as much as possible. The gas gun was pressurized to 30 psi for every experiment, corresponding to a strain rate in the samples of approximately 2000 s^{-1}.

High-speed color photography of each experiment was captured using a Phantom v2012 camera at a rate of 100,000 frames per second. Samples were backlit by an LED lamp with a piece of tissue paper used as a diffuser. The lighting and exposure settings were such that the samples were slightly overexposed in preloading conditions. This was intentional to ensure sufficient light was available as the sample was compressed and light source blocked by the bars so that the color change could still be captured. Kolsky data collection and the high-speed imagery were synced to the same optical trigger to ensure equivalent timing.

To link the activation of the embedded mechanophore to the Kolsky data, computer analysis of the high-speed imagery was used. Each individual image was cropped to show only the sample and bar, without any background. Small sample regions were manually selected of the black bar area and lighter sample area. Then, each pixel in each examined image was classified as either sample or bar using a nearest neighbor match. Finally, the average color of the pixels that was determined to be part of the sample in each image was recorded. CIELAB color space was used for this portion of the analysis, as rather than the typical red, green, and blue (RGB) channels of RGB color space, it separates the color channels into blue–orange, red–green, and illumination. CIELAB color space also provides the benefit of reducing the effects of illumination on recorded color change, as well as the blue–orange channel being convenient for this work as the SP-embedded PDMS tends to start out yellow–orange and turn blue under load. This method was used rather than

simply designating a manual region to track throughout the experiment because the sample undergoes significant deformation during compression; any manually designated region would by necessity be very small and not representative of the behavior of the entire sample.

To determine activation from the recorded color history, all three channels were examined for any characteristic signal. A local minimum resulting from the decreasing light from compression of the sample as well as color change from yellow to blue was detected. This local minimum was compared with visual detection of the color change and served as a consistent, repeatable indicator. This specific trigger point has the downside of occurring several frames after activation is visible by eye. However, this delay is consistent at 5 frames (50 μs) with a margin of error of approximately ±1 frame (10 μs). For consistency, the activation point determined by computer analysis is referred to as the activation point in this report, as determining activation by eye is both difficult and somewhat subjective. However, as a result of the delay, this activation point should be considered not the exact beginning of activation but rather the point at which activation of a large portion of the mechanophore throughout the entirety of the sample has occurred. For the reasons stated, there is some error associated with the detection of the exact onset time. Further details on the high-speed imagery analysis method, minus enhancements described here, can be found in previous works by the authors.[7,9]

4. Results

Initial results indicated the peak and activation stresses and strains for each material tended to cluster around a consistent value, but with occasional outliers that made drawing conclusions difficult. These outliers are attributed to the inherent difficulty of Kolsky compression experiments on soft samples, with the primary specific cause being the difficulty of ensuring parallel loading surfaces on a soft sample. While the cutting jig was described previously and proved superior to attempting to cut parallel faces by hand, bending and deformation of the sample billets during cutting was present. In some samples, this lack of parallelism was worse than others. In typical compression experiments on metals, the effect of lack of parallelism is identifiable by a long low-stress but high-strain region on the stress–strain curve as the protruding corner of the sample is compressed until it aligns with the full thickness, and loading proceeds as in a valid test. Similarly, in brittle ceramics this issue can be identified by premature failure of the protruding corner as it takes the entirety of the loading. However, neither of these detection methods are viable for soft samples; soft elastomers do not fail like brittle ceramics and these materials inherently possess a low-stress, high-strain linear region that covers up any smaller effects from misalignment.[15,21] Instead, the irregular sample was

addressed by two separate methods. First, the high-speed imagery was checked for visible misalignment, as is done for any valid Kolsky test. However, visual detection only removes the most egregious examples; smaller degrees of misalignment may not be visible. Second, a large number of additional replicate experiments were run to give a larger sample pool for statistical analysis. Of this sample pool, the samples with the top two and bottom two peak stress measurements were omitted from the final data set. This provides a consistent omission of outlying results while not removing any large trends.

Figure 2 shows the peak stress and strain values, as well as activation stress and strain values of the final data set. Peak stress ranged from 8.7 MPa for the lowest studied temperature (23 °C) to 13.0 MPa for the highest curing temperature (138 °C). Samples cured at elevated temperatures (68, 113, and 138 °C) are all within one standard deviation of each other with respect to both peak stress and peak strain. However, the RT samples achieve significantly higher peak strain, but lower peak stress, due to their soft nature.

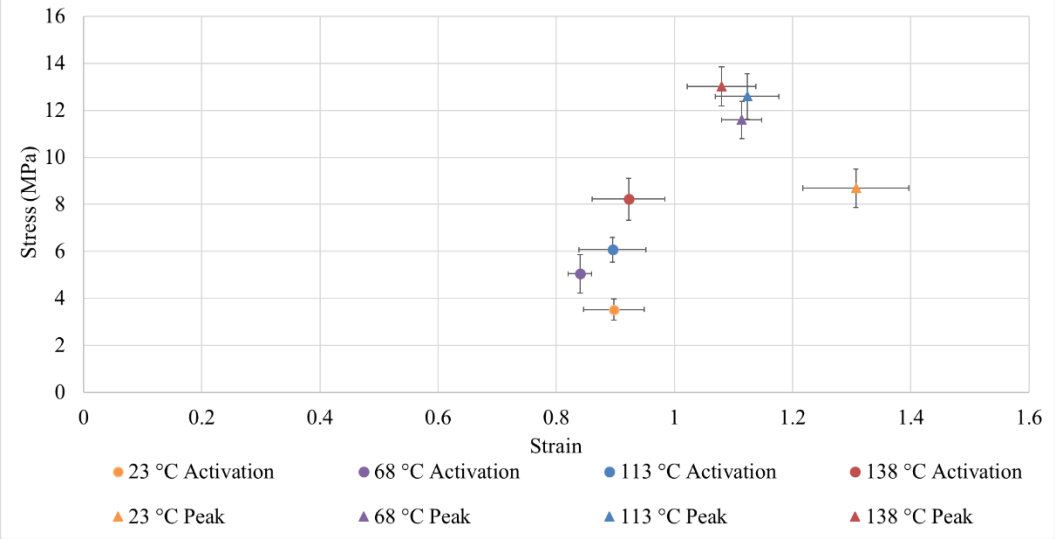

Fig. 2 Visual summary of average peak true stress and true strain and activation true stress and true strain. Error bars represent one standard deviation.

As seen in Figure 2, the onset of activation occurs well before failure, with activation and peak stresses and strains that differ by greater than one standard deviation, aside from a slight overlap between the 68 °C samples (5.0 ±0.8 MPa) and the 113 °C samples (6.1 ±0.5 MPa). The RT samples require the least stress to activate the SP mechanophore, likely due to the softer nature of the bulk elastomer produced at this temperature. Note that all stresses and strains are true stresses and strains (Table 1).

Table 1 Summary of average peak true stress and true strain and average activation true stress and true strain. The margin of error shown represents one standard deviation.

Curing temperature (°C)	Peak strain	Peak stress (MPa)	Strain at activation point	Stress at activation point (MPa)
23 (RT)	1.31 ± 0.09	8.7 ± 0.8	0.90 ± 0.05	3.5 ± 0.5
68	1.11 ± 0.03	11.6 ± 0.8	0.84 ± 0.02	5.0 ± 0.8
113	1.12 ± 0.05	12.6 ± 1.0	0.90 ± 0.06	6.1 ± 0.5
138	1.08 ± 0.06	13.0 ± 0.8	0.92 ± 0.06	8.2 ± 0.9

5. Discussion

On examining the results summarized in Fig. 2 and Table 1, the activation strain does not seem to be affected by the curing temperature, contrary to what was anticipated. The stress values at the onset of mechanochromism seem to increase as the curing temperature is increased. This finding confirms the previously observed trend[13] that as the network cross-linking density is increased, higher levels of stress occur at the onset of mechanochromism. The combination of consistent activation strain and varying activation stress suggests that activation is strain controlled: when a sample under compression reaches the critical strain around 0.90, the SP mechanophore activates regardless of the stress needed to reach that critical strain.

The peak stresses and strains are all clustered within a standard deviation of each other, except for the RT samples. This shows the RT samples are significantly softer than the rest, but after reaching a curing temperature of, at most, 68 °C, there seems to be only a small effect on the bulk properties of the PDMS from further increase of the curing temperature. This is a notable difference from the activation behavior, which continues to show variance with curing temperature at the higher temperatures measured. This result does match the study by Johnston et al. that saw very similar compressive behavior, with the difference between curing temperatures at 100 °C and 125 °C being much smaller than a similar range at lower temperatures.[15]

The results are consistent with the following picture. Activation of a given mechanophore within the sample is determined by the tension in a mechanophore-bearing strand or cross link. That tension is in turn a function of the ratio of the actual end-to-end distance of the mechanophore-bearing strand to its fully extended contour length; the larger the end-to-end distance, the greater the tension in the strand. The ratio of initial end-to-end distance to contour length in the as-cured

network further depends on the length of the strand (either the actual length of the physical strand itself in the affine model, or the effective length of the phantom chain in the non-affine models of elasticity). Longer strands have a lower initial ratio and are expected to require a greater stretch to activate. The independence of onset strain as a function of extent of curing suggests the most easily activated mechanophore strands are essentially identical at early stages of curing as compared to more complete stages of curing. Because the current analysis considers only the onset strain, this need not apply to all mechanophores in the network, just those necessary to achieve threshold detection. The key point is mechanophore activation necessarily reports on the local strain of a subset of mechanophore-embedded strands, which is correlated with the total strain of the sample.

In contrast, the activation stress reports on both the stress contributed by the activating strands and the stress contributed by the rest of the bulk network. At higher curing temperatures, a greater number of elastically active chains are formed, and so the total stress within the network is greater at a given strain—even though contributions from a given mechanophore-bearing strand is the same. Put another way, the mechanochromic strand must be stretched to a certain point to activate, and it takes a greater load to strain the sample to that point when the network is cured to a greater extent.

6. Conclusions

This work divulged the effects of curing temperature variation on the activation (SP-to-MC transition with accompanying color change) of SP-embedded PDMS. It was found that the strain needed for activation remained similar for the four curing temperatures studied. The relatively consistent activation strains would indicate that activation of the SP mechanophore is strain controlled, requiring a strain of approximately 0.90 to induce the SP-to-MC transition. As the curing temperature increases, the average molecular weight between cross links decreases, the network cross-linking density increases, and the theoretical stretchability decreases. This in turn requires higher levels of stresses acting on the C–O bond at the onset strain. Our results indicate that greater stresses are required for onset of mechanochromism as the curing temperature was increased, therefore following the same trend. Furthermore, since the onset strains did not vary much with the curing temperature, our results seem to indicate that network cross-linking density effects and/or stretchability effects are subdued under higher strain rate loadings. To provide a more thorough characterization of the behavior of SP-embedded PDMS, future work should include quasi-static experiments conducted at the aforementioned temperatures to compare to the high strain rate results reported here.

7. References

1. Potisek SL, Davis DA, Sottos NR, White SR, Moore JS. Mechanophore-linked addition polymers. J Am Chem Soc. 2007;129(45):13808–13809.
2. Zhang Y, Lund E, Gossweiler GR, Lee B, Niu ZN, Khripin C, Munch E, Couty M, Craig SL. Molecular damage detection in an elastomer nanocomposite with a coumarin dimer mechanophore. Macromol Rapid Commun. 2021;42:2000359.
3. Stratigaki M, Gostl R. Methods for exerting and sensing force in polymer materials using mechanophores. ChemPlusChem 2020;85(6):1095–1103.
4. Diesendruck CE, Moore JS. Mechanophores for self-healing applications. In: Binder WH, editor. Self-healing polymers: from principles to applications. Wiley-VCH Verlag GmbH & Co; 2013.
5. Lin Y, Kouznetsova TB, Craig SL. A latent mechanoacid for time-stamped mechanochromism and chemical signaling in polymeric materials. J Am Chem Soc. 2020;142(1):99–103.
6. Hu X, Zeng T, Husic CC, Robb MJ. Mechanically triggered small molecule release from a masked furfuryl carbonate. J Am Chem Soc. 2019;141(38):15018–15023.
7. Shannahan L, Berry J, Lin Y, Barbee M, Craig S, Casem D, Fermen-Coker M. A mechanochemistry-based technique for early material damage detection in high strain rate processes. Army Research Laboratory (US); 2019 Jan. Report No.: ARL-TR-8629.
8. Lin Y, Barbee MH, Chang CC, Craig SL. Regiochemical effects on mechanophore activation in bulk materials. J Am Chem Soc. 2018;140(46):15969–15975.
9. Shannahan L, Lin Y, Berry J, Barbee M, Craig S, Fermen-Coker M, Craig S. Onset of mechanochromic response in the high strain rate uniaxial compression of spiropyran embedded silicone elastomers. Macromol Rapid Commun. 2021;42(1):2000449.
10. Barbee MH, Kouznetsova T, Barrett SL, Gossweiler GR, Lin Y, Rastogi SK, Brittain WJ, Craig SL. Substituent effects and mechanism in a mechanochemical reaction. J Am Chem Soc. 2018;140(40):12746–12750.

11. Watabe T, Ishizuki K, Aoki D, Otsuka H. Mechanochromic dendrimers: the relationship between primary structure and mechanochromic properties in the bulk. Chem Comm. 2019;55(48):6831–6834.

12. Berry J, Lin Y, Shannahan L, Fermen-Coker M, Craig SL. Synthesis of a functionalized, multi-arm spiropyran mechanophore and evaluation under quasi-static and high-rate loading conditions in bulk PDMS. DEVCOM Army Research Laboratory (US); 2020 Sep. Report No.: ARL-TR-9086.

13. Xia Z, Alphonse VD, Trigg DB, Harrigan TP, Paulson JM, Luong QT, Lloyd EP, Barbee MH, Craig SL. Seeing strain in soft materials. Molecules. 2019;24(3):542/1–542/10.

14. Ashraf KM, Wang C, Nair SS, Wynne KJ. "Big dipper" dynamic contact angle curves for Pt-cured poly(dimethylsiloxane) on a thermal gradient: inter-relationships of hydrosilylation, Si−H autoxidation, and Si−OH condensation to a secondary network. Langmuir. 2019;35(7):2747–2759.

15. Johnston ID, McCluskey DK, Tan CKL, Tracey MC. Mechanical characterization of bulk Sylgard 184 for microfluidics and microengineering. J Micromech Microeng. 2014;24(3):035017.

16. Bardelli T, Marano C, Vangosa FB. Polydimethylsiloxane crosslinking kinetics: a systematic study on the Sylgard184 comparing rheological and thermal approaches. J Appl Polym Sci. 2021;138(39):51013.

17. Jo JY, Jang HG, Jung YC, Lee DC, Kim J. Revealing the dependence of molecular-level force transfer and distribution on polymer cross-link density via mechanophores. ACS Macro Lett. 2019;8(8):882–887.

18. Gossweiler GR, Hewage GB, Soriano G, Wang Q, Welshofer GW, Zhao X, Craig SL. Mechanochemical activation of covalent bonds in polymers with full and repeatable macroscopic shape recovery. ACS Macro Lett. 2014;3(3):216–219.

19. Berry JF. Facile isolation of functionalized spiropyrans without recrystallization. Army Research Laboratory (US); 2018 Sep. Report No.: ARL-CR-0830.

20. Bacon C. An experimental method for considering dispersion and attenuation in a viscoelastic Hopkinson bar. Exp Mech. 1998;38(4):242–249.

21. Lee WS, Yeo KS, Andriyana A, Shee YG, Mahamd Adikan FR. Effect of cyclic compression and curing agent concentration on the stabilization of mechanical properties of PDMS elastomer. Mater Design. 2016;96: 470–475.

Appendix – Synthetic Methods

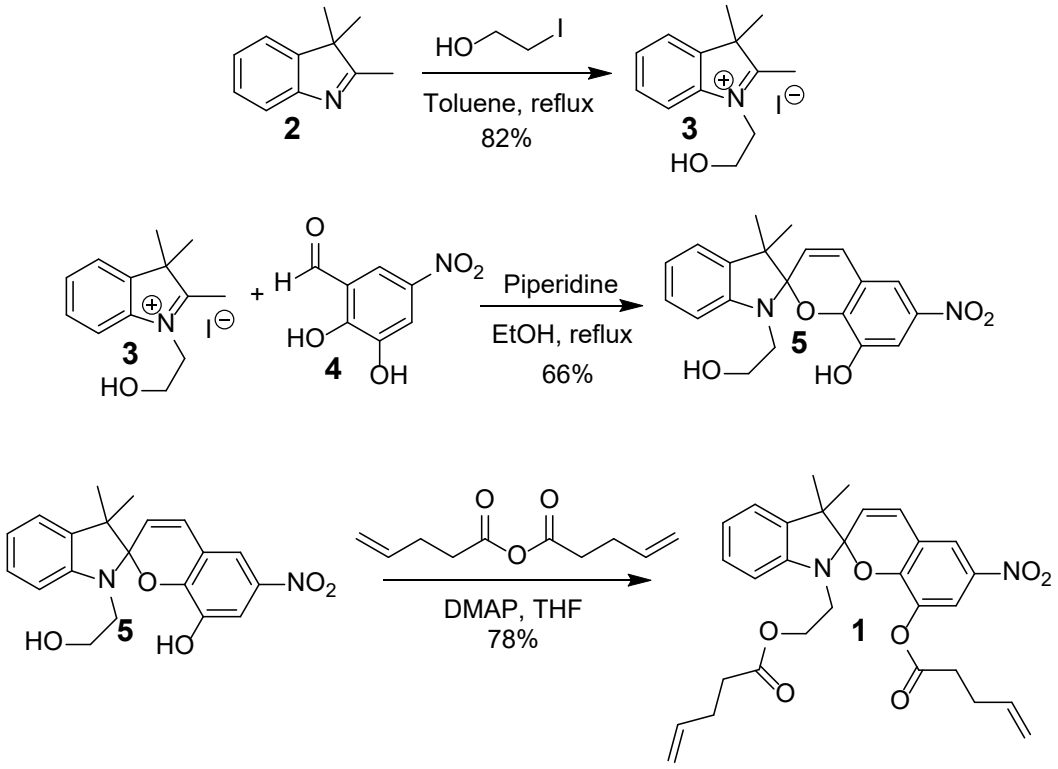

Fig. A-1 Scheme 1: the synthetic route of functionalized spiropyran 1

Most solvents were purchased from either Sigma-Aldrich or VWR International and used "as is". Absolute ethanol was purchased from Koptec, Inc. $CDCl_3$ was purchased from Sigma-Aldrich, and DMSO-d_6 was purchased from Cambridge Isotope Laboratories. All other reagents were purchased from either Sigma-Aldrich or Alfa Aesar. All glassware was dried in an oven set to 110 °C, and reactions were stirred magnetically under an argon atmosphere. Thin layer chromatography (TLC) was performed using EMD/Millipore Silica Gel 60 TLC plates (250 μm, F_{254} indicator) and viewed under UV light (254 nm). Column chromatography was performed using SiliCycle SiliaFlash F60 silica gel (40–63-μm particle size, 230–400 mesh). ^{1}H-NMR and ^{13}C-NMR were performed on a Bruker 400-MHz nuclear magnetic resonance (NMR) system. NMR values are reported in parts per million (ppm) as compared with the reference peaks of $CDCl_3$ (7.26 ppm for ^{1}H and 77.16 ppm for ^{13}C) and DMSO-d_6 (2.50 ppm for ^{1}H and 39.52 ppm for ^{13}C). ^{1}H-NMR values are reported as chemical shift in ppm, multiplicity, coupling constant in hertz, relative integral. ^{1}H-NMR multiplicities are indicated as s (singlet), d (doublet), t (triplet), dd (doublet of doublets), td (triplet of doublets), m (multiplet), and b (broad). EtOH is ethanol, EtOAc is ethyl acetate, DCM is dichloromethane, THF is tetrahydrofuran, PE is petroleum ether, HBr is hydrobromic acid, and $NaHCO_3$ is sodium bicarbonate.

1-(2-hydroxyethyl)-2,3,3-trimethyl-3*H*-indolium iodide (3)

Following a modified literature procedure,[1] 2-iodoethanol (7.36 mL, 94.3 mmol, 1.5 equiv.) was added dropwise over 5 min to a solution of 2,3,3-trimethyl-3*H*-indole **2** (10.0 g, 62.9 mmol, 1 equiv.) in 100 mL of toluene. The mixture was heated to reflux (bath temperature 120 °C) and stirred for 20 h. After cooling to room temperature, the mixture was further cooled to 0 °C in an ice bath, then filtered to give a dark purple solid, which was washed with ice-cold toluene. The solid was triturated several times with acetone to give 1-(2-hydroxyethyl)-2,3,3-trimethyl-3*H*-indolium iodide **3** (17.08 g, 82% yield) as a light-pink solid. ^{1}H-NMR and ^{13}C-NMR were in agreement with the previously reported material.[1] ^{1}H-NMR (400 MHz, DMSO-d_6) δ 7.97-7.94 (m, 1H), 7.86-7.84 (m, 1H), 7.64-7.60 (m, 2H), 4.60 (t, J = 5.0 Hz, 2H), 3.88 (t, J = 5.0 Hz, 2H), 2.82 (s, 3H), 1.55 (s, 6H). ^{13}C-NMR (100 MHz, DMSO-d_6) δ 197.8, 141.8, 141.1, 129.3, 128.8, 123.4, 115.6, 57.8, 54.2, 50.2, 22.0, 14.4.

2,3-dihydroxy-5-nitrobenzaldehyde (4)

Following the literature procedure,[2] 90 mL of 48% aq. HBr was added to 2-hydroxy-3-methoxy-5-nitrobenzaldehyde (5.00 g, 25.4 mmol, 1 equiv.) in a round-bottom flask and heated to 140 °C for 5.5 h. After cooling to room temperature, the reaction mixture was added to 120 mL of cold water. The suspension was filtered and washed with water to give a brown solid. This solid was dissolved in 150 mL of hot EtOAc, activated carbon was added and, after brief stirring, the solution was passed through a small plug of silica gel. The filtrate was then placed into a –40 °C freezer to cool overnight. The precipitated solids were filtered off to give 2,3-dihydroxy-5-nitrobenzaldehyde **4** as light-yellow needles. Additional product was obtained through rotary evaporation of the supernatant. Total yield was 3.27 g, 70% yield. ^{1}H-NMR and ^{13}C-NMR matched that of the previously reported material.[2] ^{1}H-NMR (400 MHz, DMSO-d_6) δ 11.18 (bs, 2H), 10.30, (s, 1H), 7.98 (d, J = 2.8 Hz, 1H), 7.78 (d, J = 2.8 Hz, 1H). ^{13}C-NMR (100 MHz, DMSO-d_6) δ 189.8, 156.0, 147.2, 139.2, 121.8, 114.6, 113.2.

---

[1] Gossweiler GR, Hewage GB, Soriano G, Wang Q, Welshofer GW, Zhao X, Craig SL. Mechanochemical activation of covalent bonds in polymers with full and repeatable macroscopic shape recovery. ACS Macro Lett. 2014;3(3):216–219.

[2] Hemmer JR, Smith PD, van Horn M, Alnemrat S, Mason BP, de Alaniz JR, Osswald S, Hooper JP. High strain-rate response of spiropyran mechanophores in PMMA. J Poly Sci, Part B: Poly Phys. 2014;52(20):1347–1356.

1'-(2-hydroxyethyl)-3',3'-dimethyl-6-nitrospiro[chromene-2,2'-indolin]-8-ol (5)

Following a slightly modified literature procedure,[1] 1-(2-hydroxyethyl)-2,3,3-trimethyl-3*H*-indol-1-ium iodide **3** (2.71 g, 8.19 mmol, 1 equiv.) and 2,3-dihydroxy-5-nitrobenzaldehyde **4** (1.50 g, 8.19 mmol, 1 equiv.) were combined in a round-bottom flask along with 82 mL of absolute EtOH. Piperidine (1.62 mL, 16.4 mmol, 2 equiv.) was added dropwise over 5 min with stirring, and the mixture turned black. The flask was then heated (oil bath) to 100 °C and stirred at this temperature for 3 h. The mixture was removed from the oil bath and cooled to room temperature, then further cooled to 0 °C in an ice bath and filtered to give a black solid. The filtered solid was washed with small aliquots of ice-cold EtOH to give 1'-(2-hydroxyethyl)-3',3'-dimethyl-6-nitrospiro[chromene-2,2'-indolin]-8-ol **5** (2.01 g, 66% yield) as an emerald-green solid. This material was used directly without purification.

3',3'-dimethyl-6-nitro-1'-(2-(pent-4-enoyloxy)ethyl)spiro[chromene-2,2'-indolin]-8-yl pent-4-enoate (1)

Following a modified literature procedure,[3] a mixture of 1'-(2-hydroxyethyl)-3',3'-dimethyl-6-nitrospiro[chromene-2,2'-indolin]-8-ol **5** (0.55 g, 1.51 mmol, 1 equiv.) and 4-dimethylaminopyridine (DMAP, 0.018 g, 0.15 mmol, 0.1 equiv.) was combined with 8 mL of dry THF and stirred for 5 min. 4-Pentenoic anhydride (0.62 mL, 3.41 mmol, 2.25 equiv.) was added dropwise at room temperature over 5 min. The solution changed from blue to purple and was stirred for 96 h at room temperature. THF was removed via rotary evaporation, then the purple residue was dissolved in 80 mL DCM. The organic layer was washed sequentially with 40 mL saturated $NaHCO_3$, 40 mL 1N HCl, 40 mL water, and 40 mL brine. After drying with Na_2SO_4, the solvent was removed under reduced pressure. Column chromatography using a solvent system ranging from 3% EtOAc/PE to 6% EtOAc/PE was used to elute the product from the column. The fractions containing product (product R_f = 0.81 in 3:1 PE:EtOAc) were combined, and solvent was removed (through rotary evaporation) until the solution started turning a darker shade of blue (about 10% of original volume). Petroleum ether (PE; ~200 mL) was then added to the solution and stirred. After removing some of the solvent under reduced pressure, the solution turned a bright-yellow color and the product precipitated out as a yellow solid. The remaining solvent was removed, and the product was triturated with PE and filtered to give 3',3'-dimethyl-6-nitro-1'-(2-

[3] Berry JF. Facile isolation of functionalized spiropyrans without recrystallization. Army Research Laboratory (US); 2018 Sep. Report No.: ARL-CR-0830.

(pent-4-enoyloxy)ethyl)spiro [chromene-2,2'-indolin]-8-yl pent-4-enoate **1** (631 mg, 78% yield) as a bright-yellow powder. ^{1}H-NMR and ^{13}C-NMR were in agreement with the previously reported material.[3] ^{1}H-NMR (400 MHz, $CDCl_3$) 7.94 (d, J = 2.6 Hz, 1H), 7.82 (d, J = 2.6 Hz, 1H), 7.16 (td, J = 7.7, 1.1 Hz, 1H), 7.06 (dd, J = 7.3, 1.0 Hz, 1H), 6.96 (d, J = 10.4 Hz, 1H), 6.86 (td, J = 7.5, 1.0 Hz, 1H), 6.65 (d, J = 7.8 Hz, 1H), 5.96 (d, J = 10.4 Hz, 1H), 5.82-5.71 (m, 1H), 5.61-5.49 (m, 1H), 5.04-4.86 (m, 4H), 4.28-4.10 (m, 2H), 3.33 (t, J = 6.1 Hz, 2H), 2.38-2.30 (m, 4H), 2.25-2.10 (m, 2H), 1.88-1.83 (m, 2H), 1.26 (s, 3H), 1.18 (s, 3H). ^{13}C-NMR (100 MHz, $CDCl_3$) δ 172.9, 170.5, 150.9, 146.7, 140.4, 137.8, 136.6, 136.4, 135.9, 128.5, 127.9, 121.7, 121.6, 120.3, 120.2, 119.3, 119.3, 115.7, 115.6, 107.5, 107.2, 62.6, 52.3, 42.6, 33.6, 33.0, 28.8, 28.4, 26.0, 19.5.

List of Symbols, Abbreviations, and Acronyms

1-D	one-dimensional
C	carbon
DCM	dichloromethane
DMAP	4-dimentylaminopyridine
DMSO	dimethylsulfoxide
EtOAc	ethyl acetate
EtOH	ethanol
HBr	hydrobromic acid
HCl	hydrochloric acid
LED	light-emitting diode
MC	merocyanine
$NaHCO_3$	sodium bicarbonate
NMR	nuclear magnetic resonance
O	oxygen
PDMS	polydimethylsiloxane
PE	petroleum ether
PMMA	poly(methyl methacrylate)
ppm	parts per million
RGB	red, green, blue
RT	room temperature
SP	spiropyran
THF	tetrahydrofuran
TLC	thin layer chromatography
UV	ultraviolet

1 (PDF) DEFENSE TECHNICAL INFORMATION CTR
DTIC OCA

1 (PDF) DEVCOM ARL
FCDD RLD CL
TECH LIB

1 (PDF) APPL PHYSICS LABORATORY
Z XIA

4 (PDF) NATICK SOLDIER RES DEV ENG CTR
S FILOCAMO
C DOONA
T TIANO
B FASEL

1 (PDF) DUKE UNIVERSITY
S CRAIG

2 (PDF) UNIV ILLINOIS URBANA CHAMPAIGN
J MOORE
N SOTTOS

1 (PDF) UNIVERSITY OF WISCONSIN
AJ BOYSTON

1 (PDF) UCSD
N BOECHLER

24 (PDF) DEVCOM ARL
FCDD RLD
P BAKER
FCDD RLR EM
D POREE
FCDD RLW
J ZABINSKI
S KARNA
A RAWLETT
S SCHOENFELD
J CIEZAK-JENKINS
FCDD RLW B
C HOPPEL
FCDD RLW M
E CHIN
FCDD RLW MA
R LAMBETH
E WETZEL
T PLAISTED
FCDD RLW MG
J LENHART
J ORLICKI
FCDD RLW P
R FRANCART
FCDD RLW PC
J BERRY
M FERMEN-COKER
L SHANNAHAN
D CASEM
J CAZAMIAS
J CLAYTON
C WILLIAMS
S TURNAGE
FCDD VTM
A HALL